Environ Earth Sci (2016) 75:443
DOI 10.1007/s12665-015-5025-z

ORIGINAL ARTICLE

Subsurface cavity detection over Patherdih colliery, Jharia Coalfield, India using electrical resistivity tomography

Abhay Kumar Bharti[1] · S. K. Pal[1] · Piyush Priyam[1] · Sahadev Kumar[1] · Shalivahan Srivastava[1] · Pramod Kumar Yadav[1]

Received: 29 November 2014 / Accepted: 21 September 2015 / Published online: 3 March 2016

Abstract The present study deals with delineation and mapping of subsurface voids which are very common around the Patherdih colliery of Jharia coal field, India. These are caused by coal fire and old unplanned/illegal mining activity. Initially, a conceptual model of void formation associated with coal fire has been proposed. The burning of coal leads to the void formation due to volume reduction because of transformation of coal to ashes. It is supposed to have significant resistivity contrasts between bedrock i.e. mainly sandstone/clay stone/shale etc. and void space, which are filled with ashes generated from burned coal seam. Field situations have been simulated through forward modeling and the data generated by gradient and dipole–dipole arrays have been corrupted by 5 % noise. The simulations have been carried out for two voids with varied resistivity. The inversions of the data for both the arrays bring up the dimension of the void within reasonable accuracy unlike its resistivity. In fact, the considered resistive void seems to be a conducting void. In the present study, data have been collected by a state-of-the-art FlashRES-Universal electrical resistivity tomography (ERT) instrument, which have 61-channel and 64 electrode data acquisition capacity. ERT sections have been generated over two profiles using Wenner, Schlumberger, gradient, dipole–dipole and joint inversion of all combine arrays. Different resistive anomalous features with resistivity of about 300–200 Ωm have been delineated in both profiles. These are associated with voids at the depths of about 23–25 and 45–54 m generated by burning of coal seams XIVA and XIV, respectively. The obtained results are in broad agreement with the available litholog and surface manifestation of coal fire. The results prove the efficacy of the ERT technique for detection of voids associated with coal fire.Author names: Please confirm if the author names are presented accurately and in the correct sequence (given name, middle name/initial, family name). Also, kindly confirm the details in the metadata are correct.it is correct

Keywords Coal fire · Cavity · Electrical resistivity tomography · Patherdih colliery

Introduction

The Jharia coalfield, India is known for its high grade coal and associated coal fires. This coalfield hosts the maximum number of known coalmine fires among all the coalfields in India, which is burning in underground since nearly a century. Jharia coalfield was nationalized in 1970 and the coal fire has spread in many areas. Unplanned coal exploitation without fire-prevention arrangements prior to the nationalization was responsible for these fires (Vaish and Pal 2013, 2015a, 2016). The unplanned old mining of the area has raised some serious geotechnical concerns viz, foundation problems on buildings placed on these mining areas and the damage to roads resulting in potholes, etc (Pal et al. 2016; Bharti et al. 2014, 2015; Kumar et al. 2015; Singh 2015; Srivardhan et al. 2016). The old mining infrastructure facilities such as shafts, mining wells, mining goaf, mining galleries, and hidden mining holes are potential locations of hazards to those who are unaware of the existence of cavities. The hazard may be caused due to the collapse of the mining cavities from natural alteration processes during the course of time by wear and tear.

The term subsurface cavity is used to denote all subsurface features such as caves, caverns, voids, karst, pothole, and sinkhole etc. The voids, potholes, and sinkholes are very

✉ S. K. Pal
sanjitism@gmail.com

[1] Department of Applied Geophysics, Indian School of Mines, Dhanbad 826004, India

common in Jharia coalfield, which are caused by coal fire and old unplanned/illegal mining activity. Underground hidden cavity pose a great threat to the local environment, agricultural land, ecology and the health of those living in their proximity; eventually resulting in loss to the national economy.

Generally, the delineation and mapping of subsurface cavities remain a challenging task in many scientific and environmental fields (Van Schoor 2002; Abu-Shariah 2009). The traditional commercial techniques use drilling to locate cavities. A much more effective and economic solution is the use of geophysical survey, which helps in optimizing the location of drill hole. The geophysical techniques used for cavity detection are (1) induced polarization tomography (Brown et al. 2011; Martínez-Moreno et al. 2014 among others), (2) 2D electrical resistivity tomography (Zhou et al. 2004; Cardarelli et al. 2006, 2010; Pánek et al. 2010; Martínez-Pagán et al. 2013; Metwaly and AlFouzan 2013; Cardarelli et al. 2014 among others), (3) vertical electrical soundings (Rodríguez Castillo and Reyes Gutierrez 1992), (4) electromagnetic (Lange 1999), (5) ground penetration radar (Mochales et al. 2008; Leucci and De Giorgi 2010; Brown et al. 2011 among others), (6) self potential (Lange 1999), (7) magnetometry (Mochales et al. 2008 among others), (8) magnetic resonance sounding (Guérin et al. 2009), (9) gravimetry (Lange 1999; Mochales et al. 2008 and Gambetta et al. 2011 among others), (10) seismic methods: seismic refraction tomography (Guérin et al. 2009; Valois et al. 2010; Cardarelli et al. 2010, 2014 among others) .

The electrical resistivity tomography (ERT) method has wide applications in environmental, engineering and shallow subsurface investigations (Van Schoor 2002). Out of all various geophysical methods, the ERT has been proved to be very effective and suitable technique for mapping and delineation of cavities (Abu-Shariah 2009; Pánek et al. 2010; Martínez-Moreno et al. 2014; Martínez-Pagán et al. 2013; Metwaly and AlFouzan 2013). It is based on the assumption that various entities like solid bedrock, sediments, air, and water filled structures would have detectable electrical resistivity contrast relative to the host medium (Pánek et al. 2010). The present study deals with delineation and mapping of subsurface voids which are very common in and around Patherdih colliery of Jharia coal field, India.

Study area

The study area, Patherdih colliery (Fig. 1a) is situated in the southern part of the Jharia coalfield. The rock formations of Jharia coalfield unconformably overlying the Archean basement, mainly belong to the Lower Gondwana group rocks of Permian age comprising Talchir, Barakar, Barren measures and Raniganj formations, from bottom to top (Fig. 1a.). The study area lies within the geographical coordinates 23.66°N–23.67°N latitude and 86.43°E–86.44°E longitude. All the working coal seams lie in the Barakar formation of Lower Gondwana group rocks and are of early-Permian age. The rocks of Barakar formation comprises predominantly of sandstone of variable grain size, argillaceous sandstone, intercalation of sandstone and shale, carbonaceous shales, jhama, mica-peridotite and coal seams (Chandra 1992; Vaish and Pal 2015b). All parts of active coal fire zones have been covered by dumping of overburden material to prevent and combat against further exaggeration of coal fire in the surroundings.

There are 14 major coal seams in the area up to a total depth of ~700 m with varying thickness of 2 m to ~19 m. The major coal bearing seams at shallow depths are affected by fire, which are coal seam-XIVA and coal seam-XIV. The average thicknesses of these seams are 2.1 and 8.6 m. The average depths of these seams are 25 and 50 m, respectively. The seams affected by fire are partially filled up and blanketed by soil. Active fire smoke has been observed near RD 90 m of profile AA′ (Fig. 1b) with the perpendicular distance of about 15–20 m. Borehole log showing different coal seams at different depth with their physical status is shown in Fig. 2.

Methodology

The burning of coal leads to the formation of voids caused by volume reduction due to the transformation of coal to ashes. The surface displacement related to mine fires, together with mining induced subsidence leads to subsequent subsidence of overlying strata. These subsidence leads to formation of cracks and fissures. The cracks and fissures helps in creation of ventilation paths for oxygen circulation. It further supports the internal combustion thus aggravating the underground coalmine fires (Jiang et al. 2011). A conceptual model of void formation caused by coal fire is shown in Fig. 3. In the present study it is supposed to have considerable resistivity contrast between bedrock i.e. mainly sandstone/clay stone/shale etc. and void space possibly filled with ashes generated from burned coal seam. The results of laboratory measurements on the samples of coal and surrounding formation show that the sandstone and shale samples have resistivity of 100 Ωm whereas the coal samples have resistivity greater than 700 Ωm at full saturation (Verma et al. 1982). The results of field investigation show that generally, the coal bearing strata exhibit relatively high resistivities in the range of about 70–350 Ωm whereas, sandstone, sandy shale and shale contribute moderate to low resistivities in the range of about 25–100 Ωm (Verma and Bhuin 1979; Verma et al. 1982).

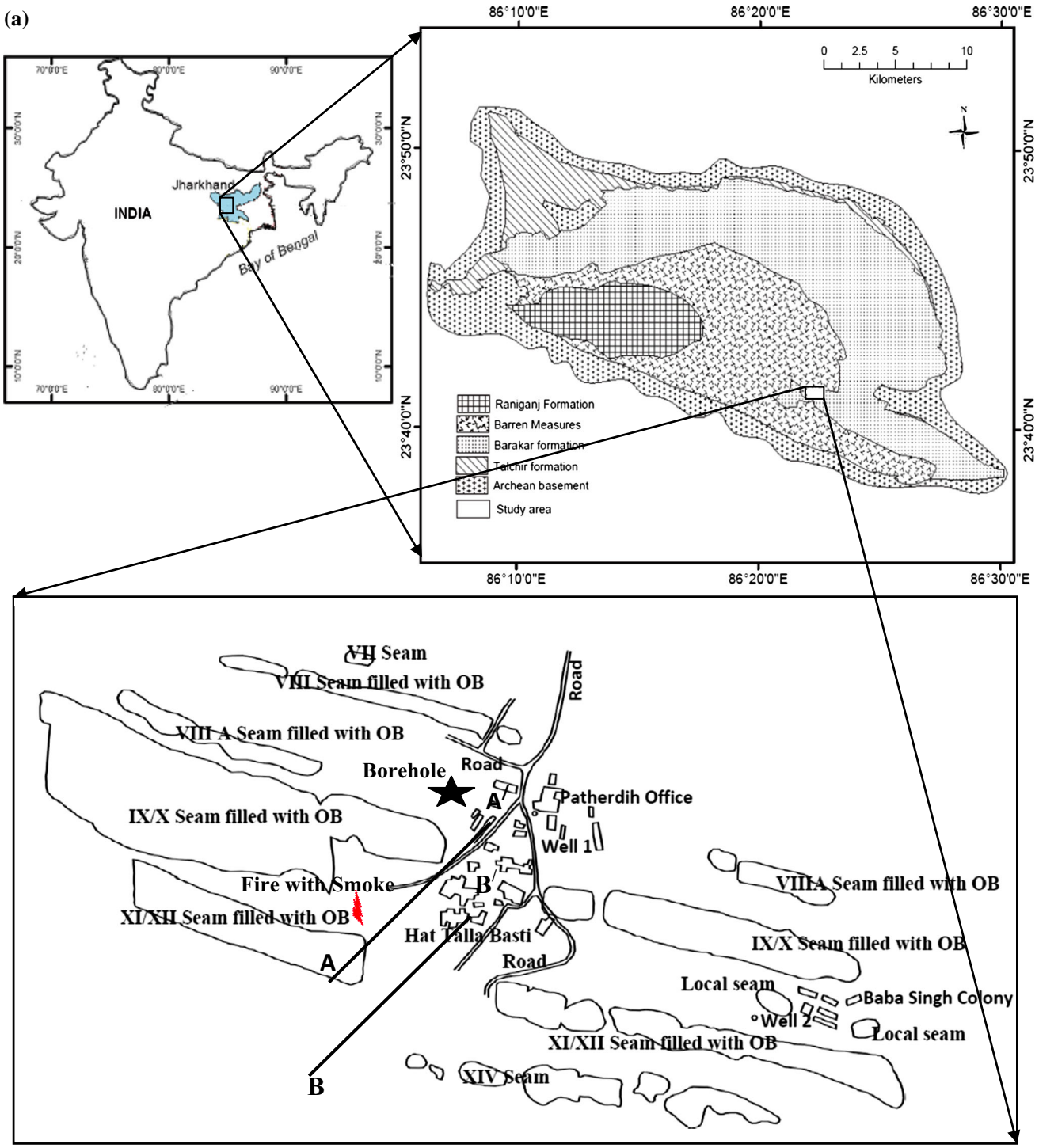

Fig. 1 **a** Location map of the study area (Patherdih colliery) along with generalized geological map of Jharia Coal field. **b** Active fire smoke has been observed near RD 90 m of AA′, the perpendicular distance is about 15–20 m from AA′

ERT data have been acquired using Wenner, Schlumberger, dipole–dipole and gradient arrays to compare the results and to delineate features using joint inversion combining all array data of same profile. These joint inversion of all array data would further optimize the resolution capability and signal-to-noise ratio (Zhou and Greenhalgh 2000; Dahlin and Zhou 2006). Among the common arrays, the Wenner array has the strongest signal

Fig. 1 continued

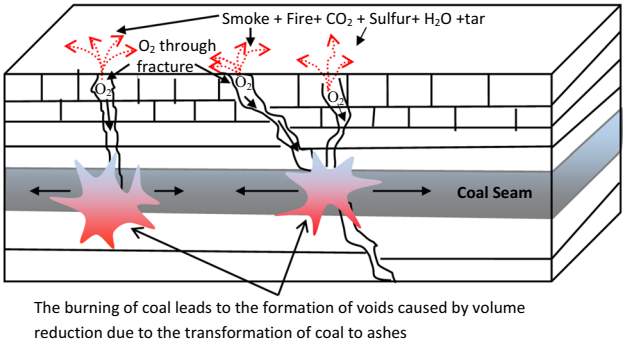

Fig. 3 A conceptual model of void formation caused by coal fire

strength. This can be an important factor if the survey is carried in areas with high background noise. Wenner array is relatively sensitive to vertical changes in the subsurface resistivity below the center of the array. However, it is less sensitive to horizontal changes in the subsurface resistivity. In general, the Wenner array is good in resolving vertical changes i.e. horizontal structures, but relatively poor in detecting horizontal changes i.e. narrow vertical structures (Loke 1999). The Schlumberger array is moderately sensitive to both horizontal and vertical structures. In areas where both types of geological structures are expected, this array might be a good compromise between the Wenner and the dipole–dipole array (Loke 1999). The dipole–dipole array is sensitive to horizontal changes in resistivity, but relatively insensitive to vertical changes in the resistivity. Thus, it is good in mapping vertical structures, such as dykes and cavities, but relatively poor in mapping horizontal structures such as sills or sedimentary layers. This array has a better horizontal data coverage than the Wenner (Loke 1999). Dahlin and Zhou (2004, 2006) have shown that the gradient array with multiple current-electrode combinations is best among the electrode arrays in terms of resolution of subsurface structures and it is clearly superior to the commonly used Wenner, Schlumberger, dipole–dipole, pole–dipole and pole–pole arrays in most of the modeled cases.

Present study utilizes a state-of-the-art 61-channel 64 electrode FlashRES-Universal electrical resistivity tomography (ERT) data acquisition system (ZZ Resistivity Imaging Pty Ltd, Australia). It offers an advanced technique for collection of data with maximum AB and MN combinations to obtain extremely large readings without being limited to standard configurations (such as Wenner, Schlumberger and dipole–dipole) than the other traditional methods. 61-channel or 61-voltage data are collected in parallel for each AB current pair and the amount of data collected reach more than 60,000 with 64-electrode layout within an hour. This is far superior to similar electric instruments in terms of the amount of data collected and data collection time. Stummer et al. (2004) performed synthetic data tests to demonstrate that the large amount of data results in better accuracy. Zhe et al. (2007) have concluded that the larger number of data points acquired using multielectrode and multichannel ERT techniques would delineate anomalies with better position, shape and accurate resistivity values after inversion. They monitored the noise through full waveform display. The additional important feature of the equipment is that there is no need to collect the data separately for different array. The user can collect the data with numbers of specified arrays in a single run and the data collected by different arrays could be used separately for interpretation. This makes data collection more effective and uses less time than the conventional systems (Zhe et al. 2007). The total 64 electrodes used for entire data acquisition system are (1) two current

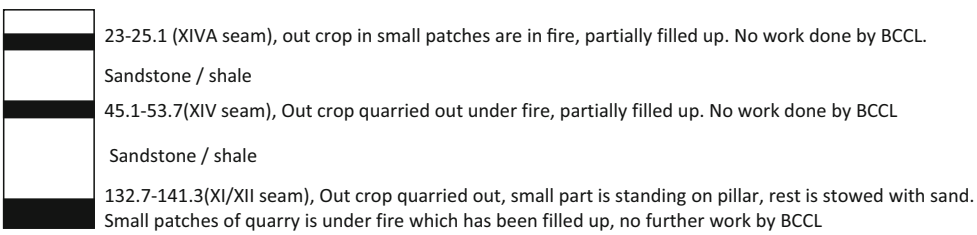

Fig. 2 Borehole log showing different coal seams at different depth with their physical status. The location of this borehole is shown in Fig. 1

Fig. 4 61 Channel ERT data acquisition field setup using 64 electrodes, of which two as current electrodes (*A*, *B*) and one as common reference electrode (M) and 61 potentials relative to M on remaining electrodes

electrodes (A and B), (2) one reference electrode (M), and (3) 61 potential electrodes (VMN1–VMN61). The principle of ERT data acquisition consists of application of constant direct current imposing into the ground via two current electrodes (A and B) and one as common reference electrode (M). It then simultaneously measures 61 potentials VMN1, VMN2…VMN61 (relative to M) on remaining 61 electrodes (Fig. 4). Position of different possible electrode pair alternatively can acts as current and remaining 61 electrode as potential electrodes keeping one electrode as common reference depending on different geometry of electrode arrays (Zhe et al. 2007). The acquired data are processed using FlashRES Universal survey data checking program for removing noisy data. The filtered output data is then inverted using a 2.5D resistivity inversion (Zhou and Greenhalgh 2000). Different anomalous resistive features observed in the inverted resistivity sections have been compared based on their approximate locations, depths, dimensions, and resistivity values (Song and Kuenzer 2014, Cardarelli et al. 2006 among others). The color scale bars of all 2D resistivity sections are given separately. The range of each color scale is 0–500 Ωm.

Results and discussions

Following, Ezersky (2008) before carrying out the survey a situation similar to the field has been simulated (Fig. 5). The sandstone of resistivity 2–80 Ωm extends from surface of the earth to 22 m. The coal seam/shaly coal of thickness 5 m overlies the sandstone of resistivity 100 Ωm at a depth of 27 m. The coal seam/shaly coal resistivity varies from 100 to 350 Ωm. Two voids of 50 m by 5 m and 40 m by 5 m at RD 160 m and RD 470 m, respectively, have been considered. The forward modeling has been carried out for two situations, (1) the resistivity of the void at RD 160 m varied from 500 to 2000 Ωm, and (2) the resistivity of the void at RD 470 m varied from 500 to 10,000 Ωm. In both the situation the considered void at RD 160 m has more resistive elements than that of RD 470 m. The forward modeling has been carried out with 10 m electrode spacing for 64 electrodes as shown in Fig. 5a. The obtained data has been corrupted with 5 % of random noise. Figure 5b, d shows the obtained results from dipole–dipole and gradient arrays for the voids with resistivity varying from 500 to 2000 Ωm. Whereas, Fig. 5c, e illustrates the results from dipole–dipole and gradient arrays with resistivity of void varying from 500 to 10,000 Ωm. Interestingly, all the results recover the void location and dimension. However, the resistivity of the void is not recovered and is about 170–300 Ωm. In fact, the resistive voids (Fig. 5a) generates conducting voids (Ezersky (2008) as shown in Fig. 5b–e. In the considered model the void at RD 160 m is more resistive than that of the RD 470 m. However, the obtained resistivity of the both the voids are approximately same.

Two ERT profiles ($AA^{/}$ and $BB^{/}$) have been considered over known fire affected area. The electrode spacing of 10 m and total profile length of 630 m have been selected for delineation and mapping of subsurface voids. The starting point i.e. 1st electrode position considered as reduced distance (RD) as 0 m (A/B) and end of the profiles i.e. 64th electrode position as RD 630 m ($A^{/}$/$B^{/}$). The ERT data have been collected using Wenner, Schlumberger, dipole–dipole and gradient arrays. Total 651, 1665, 3013 and 5368 current electrode pairs have been used for Wenner, Schlumberger, dipole–dipole and gradient arrays, respectively. The collected data have been processed using FlashRES Universal survey data checking program (FlashRES Universal, User manual 2014). The acquired data over the profiles have been processed using three different thresholds for decreasing noise level and vice versa enhancing the quality of the acquired data (FlashRES-Universal user manual). Quality factor 5 means that the 95 % of the acquired data is of good quality. Figures 6, 7 and 8 illustrates the 2D ERT sections of profile $AA^{/}$ generated using (a) Wenner, (b) Schlumberger, (c) gradient, (d) dipole–dipole and (e) joint inversion of the all combined arrays with three different thresholds viz., (1) 10 mA current and quality factor 17; (2) 40 mA current and quality factor 12 and (3) 60 mA current and quality factor 5, respectively. These thresholds correspond to 94, 84 and 43 %, respectively, of the acquired data. Similarly, 2D ERT sections of profile $BB^{/}$ with the same threshold combinations of currents and quality factors have been generated and shown in Figs. 9, 10 and 11, respectively. For this profile the above three

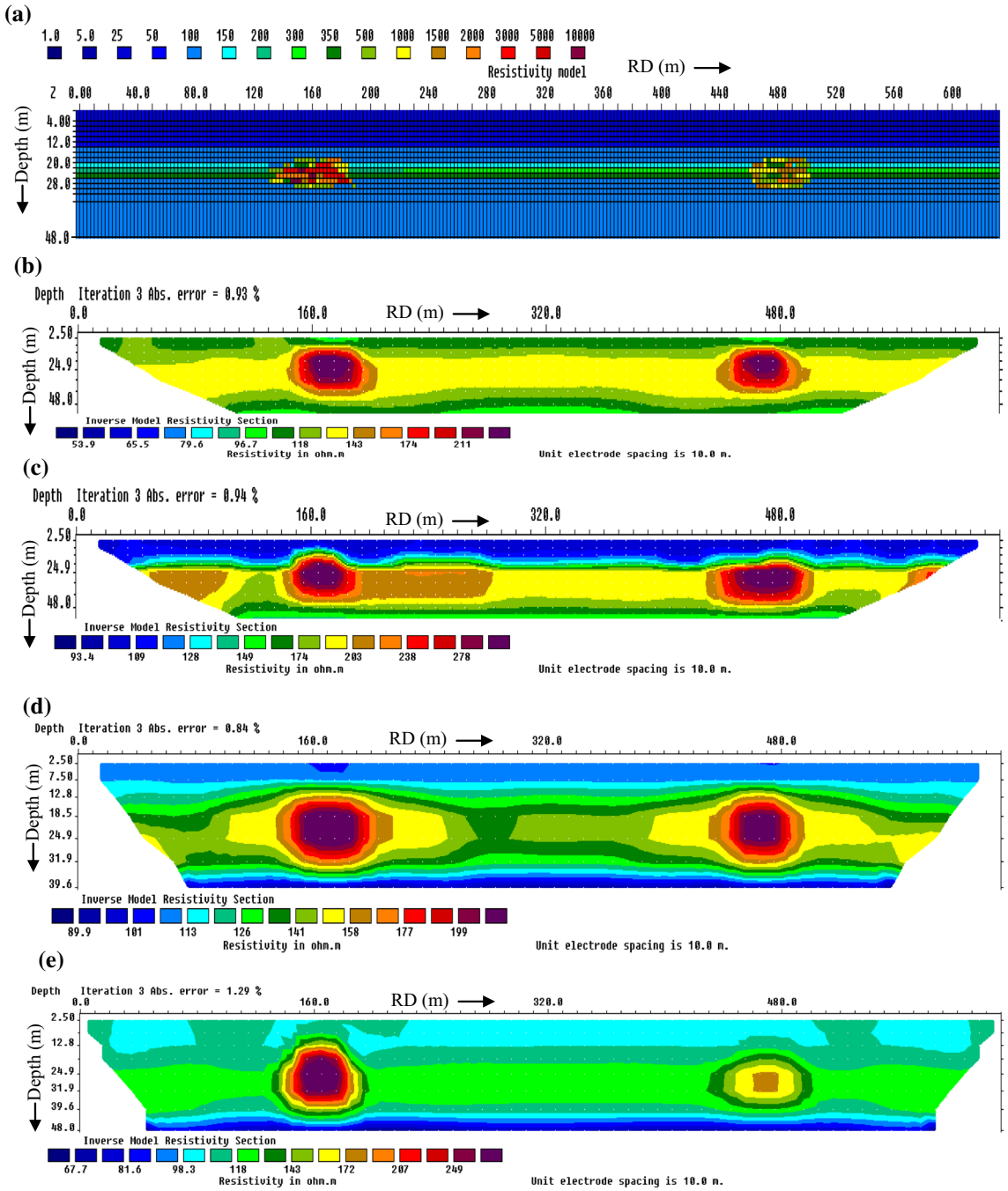

Fig. 5 **a** Resistivity model section, **b**, **d** inverse resistivity section obtained from dipole–dipole and gradient array for the void resistivity varying from 500 to 2000 Ωm, **c**, **e** inverse resistivity section obtained from dipole–dipole and gradient array for the void resistivity varying from 500 to 10,000 Ωm

thresholds corresponds to 84, 64 and 40 %, respectively, of the acquired data. The details of various features delineated from the inverted resistivity sections of various arrays have been presented in Tables 1 and 2, respectively, for both AA′ and BB′ profiles. Out of three different thresholds, the best result is obtained when the quality factor is 5 with current threshold of 60 mA. The quality of the results naturally decreases with the increase in the quality factor and decrease in the current threshold. The quality of results may changes with varying current source, but this would vary if spontaneous potential are absent which depends on environment noise. Figure 12a,

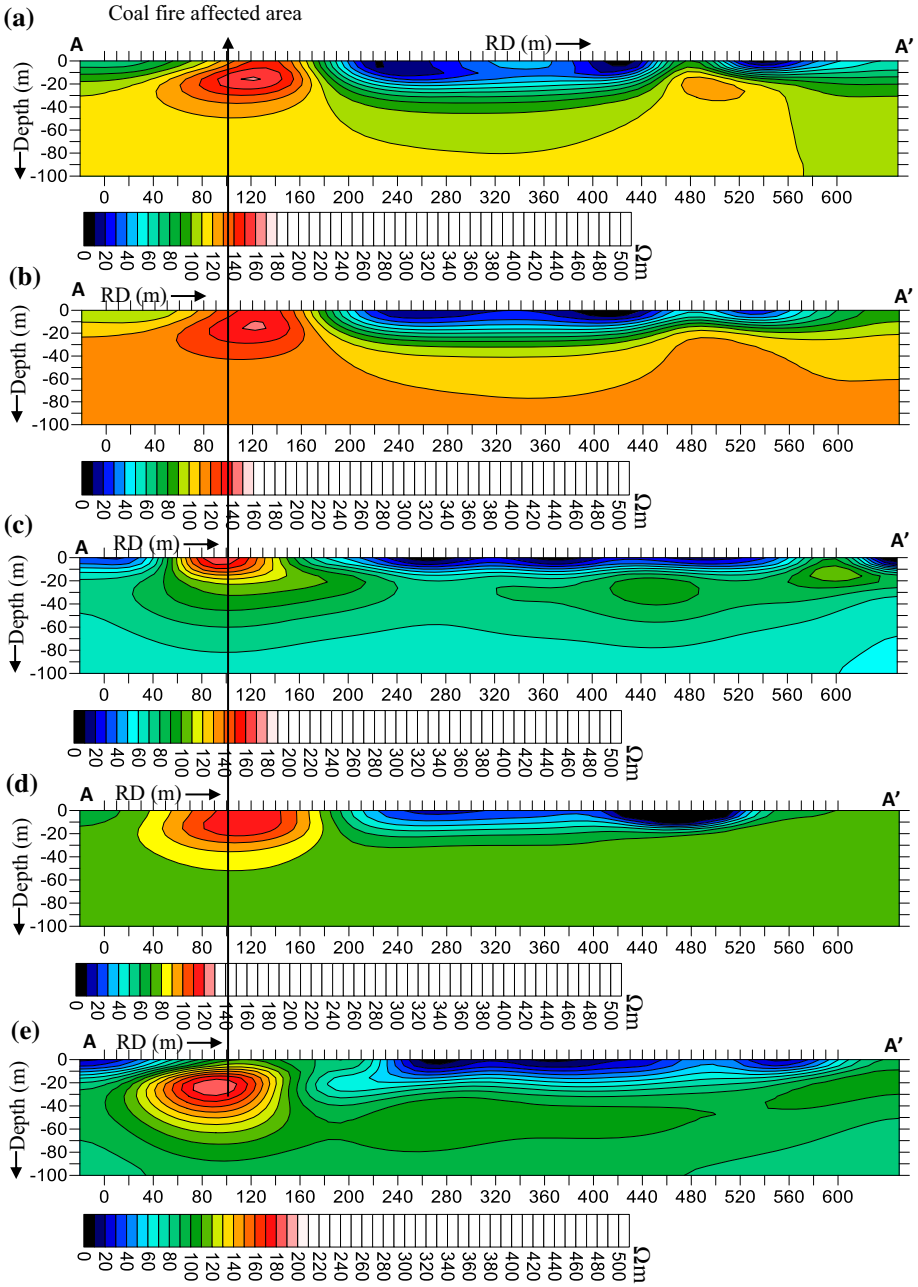

Fig. 6 2D ERT section along AA′ using **a** Wenner, **b** Schlumberger, **c** gradient, **d** dipole–dipole arrays and **e** joint inversion of all the arrays with current threshold of 10 mA and quality factor 17

b compares the root mean square (RMS) error for different arrays with three thresholds for both the profiles. Tables 1 and 2 provide the details of RMS errors of inversion results generated using different array for both the profiles. It has been observed that RMS error increases with the increase in quality factor. RMS error is minimum for the joint inversion of all the combined arrays. RMS error of the Gradient array is least of all the other arrays viz., Wenner, Schlumberger and dipole–dipole arrays.

It has been observed that the ERT data collected over profile AA′ have better current injection (proper grounding of electrodes) and low RMS error (quality factor low) of resistivity readings than that of the ERT data collected over profile BB′. Due to scarcity of space and for mapping of the feature encountered in AA′, the profile BB′ has been taken partially over rugged topography filled with overburden which could not establish proper grounding in some electrodes, despite watering with bentonite clay to the elec-

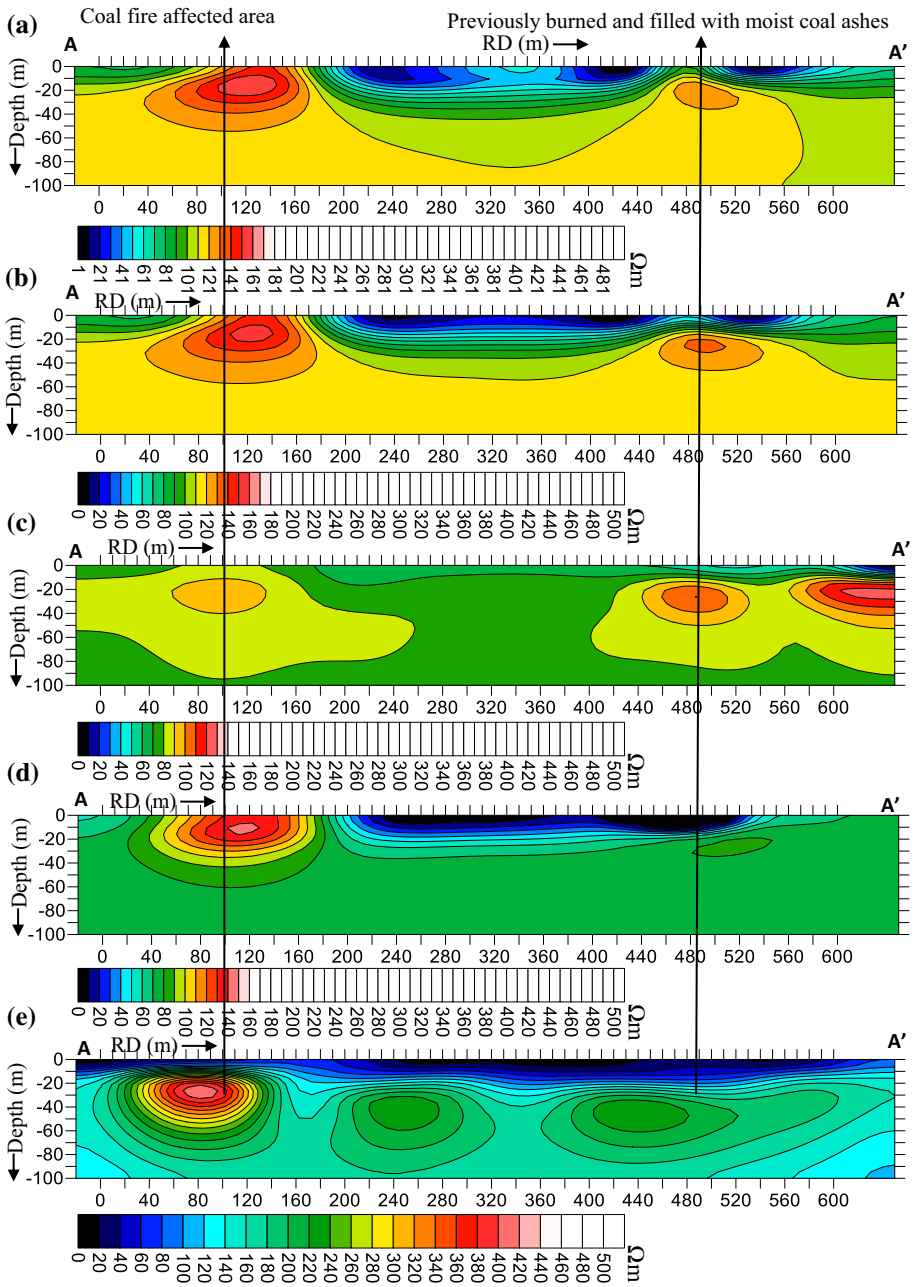

Fig. 7 2D ERT section along AA′ using **a** Wenner, **b** Schlumberger, **c** gradient, **d** dipole–dipole arrays and **e** joint inversion of all the arrays with current threshold of 40 mA and quality factor 12

trodes. It results in degradation of the data quality of the profile BB′.

The comparative study of Figs. 6, 7, 8, 9, 10, 11 and Tables 1 and 2 proves that different resistive anomalous features delineated using joint inversion of combined data collected by all arrays gives best suitable results. Because it provides 2D inverted section with minimum RMS error among all. The different anomalous resistive features delineated by this technique could be correlated well with same in all individual arrays. Similarly, it is observed that features delineated using gradient array provides next suitable results with less RMS error than the dipole–dipole, Schlumberger and Wenner arrays. Whereas, features delineated using dipole–dipole array provides second next suitable results with less RMS error than the Schlumberger and Wenner arrays.

Figures 6, 7, 8, 9, 10, and 11 shows the presence of voids associated with coal fire zone with location, dimension and resistivity. Generally, the gradient, dipole–dipole and joint inversion of all combine arrays brings up more

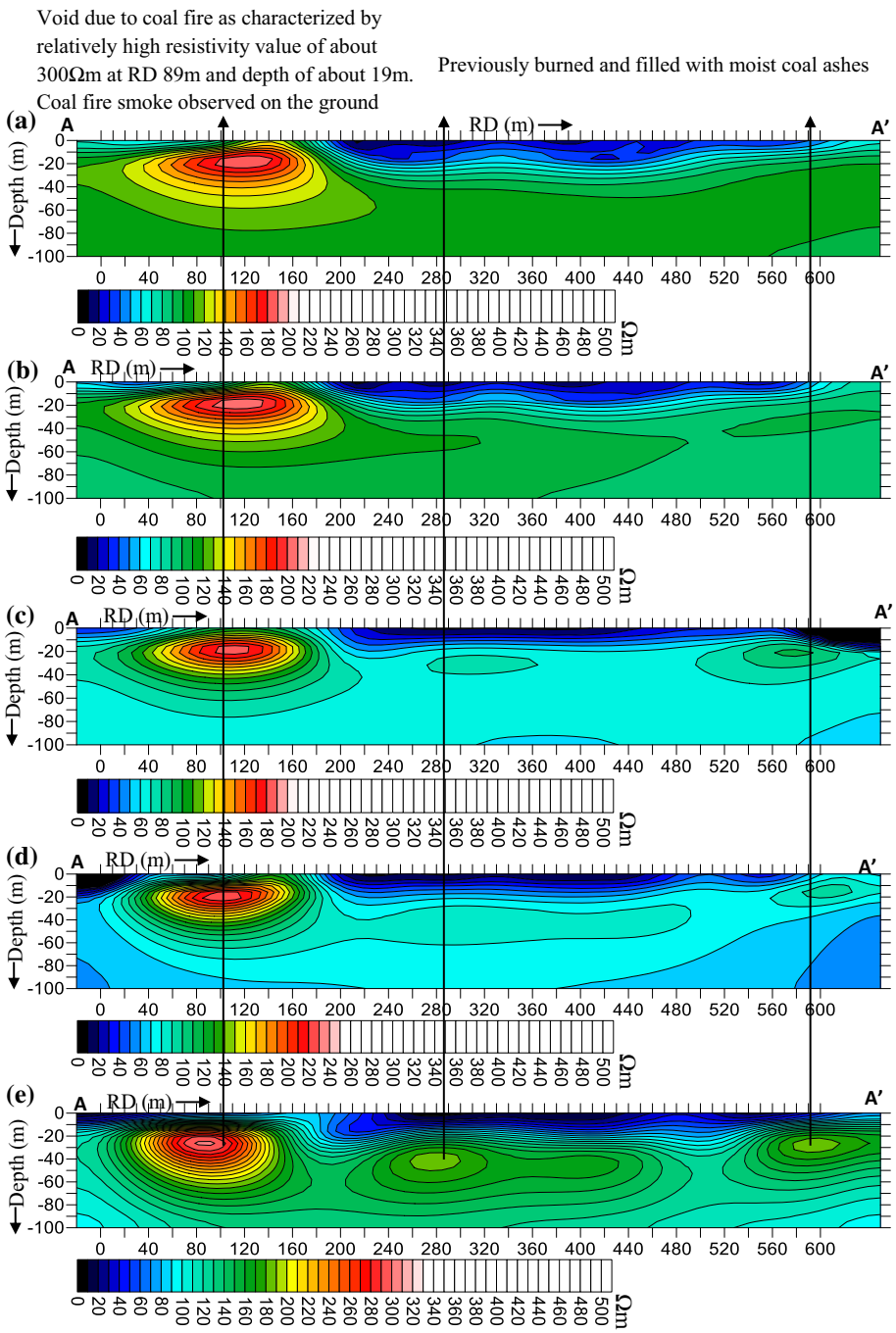

Fig. 8 2D ERT section along AA′ using **a** Wenner, **b** Schlumberger, **c** gradient, **d** dipole–dipole arrays and **e** joint inversion of all the arrays with current threshold of 60 mA and quality factor 5

than one voids associated with coal fire. The imprints of entire coal seam fires have been mapped by using joint inversion of combined array only (Figs. 6e,7e,8e,10e and 11e). The delineated voids seem to be conducting, in comparison to the results obtained of model study (Fig. 5). The observation regarding resistivity of the voids may also be related to the heating of water-saturated coal samples. Duba (1977) studied the electrical conductivity/resistivity of coal and coal char. Revil et al. (2013, Fig. 7) discussed the shape of this curve. Initially, a large increase of resistivity from 1000 Ωm at 24 °C to $\sim 6.3 \times 10^8$ Ωm at 110 °C is observed (Duba 1977). Then the resistivity reaches to $\sim 3.1 \times 10^9$ Ωm at 300 °C with a relatively smooth increment owing to water loss on drying or desaturation (Revil et al. 2013). Subsequently, resistivity decreases slowly to $\sim 2.5 \times 10^6$ Ωm at 515 °C and then decreases rapidly to ~ 0.01 Ωm at 800 °C. Revil et al. (2013) termed this path as dry path.

The voids delineated at depth of about 23–25 m is caused by XIVA coal seam fire. Whereas voids

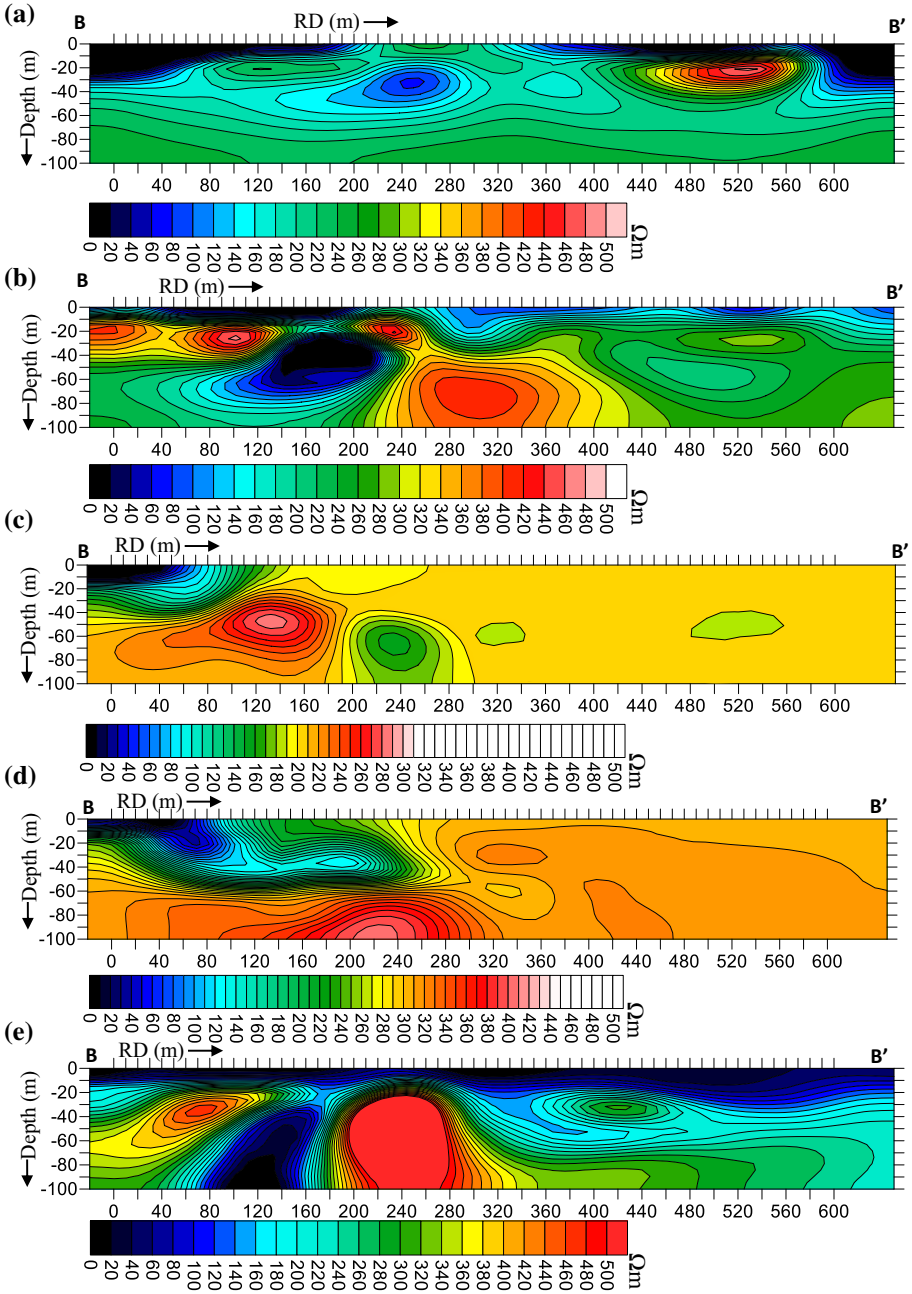

Fig. 9 2D ERT section along BB′ using **a** Wenner, **b** Schlumberger, **c** gradient, **d** dipole–dipole arrays and **e** joint inversion of all the arrays with current threshold of 10 mA and quality factor 17

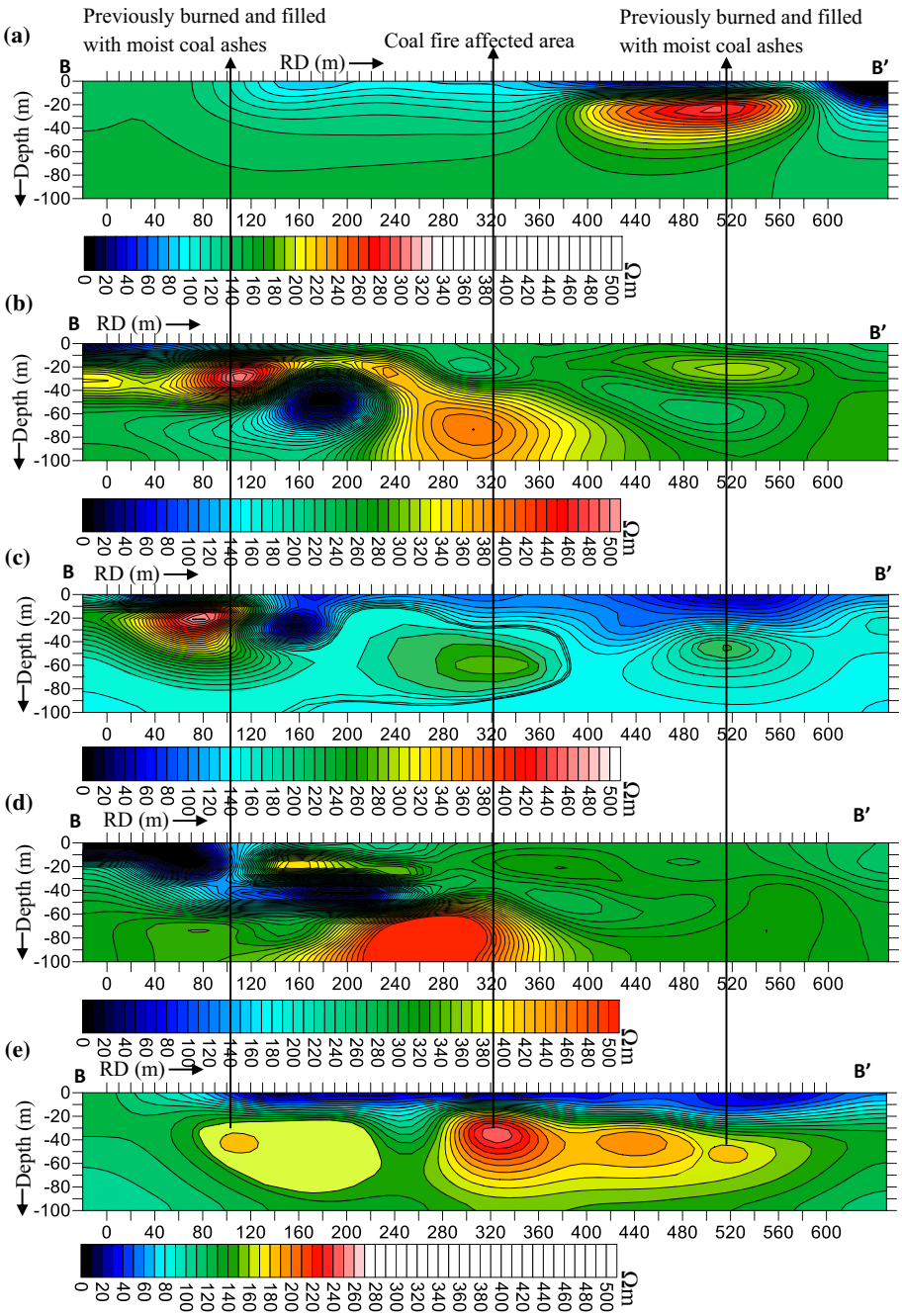

Fig. 10 2D ERT section along BB′ using **a** Wenner, **b** Schlumberger, **c** gradient, **d** dipole–dipole arrays and **e** joint inversion of all the arrays with current threshold of 40 mA and quality factor 12

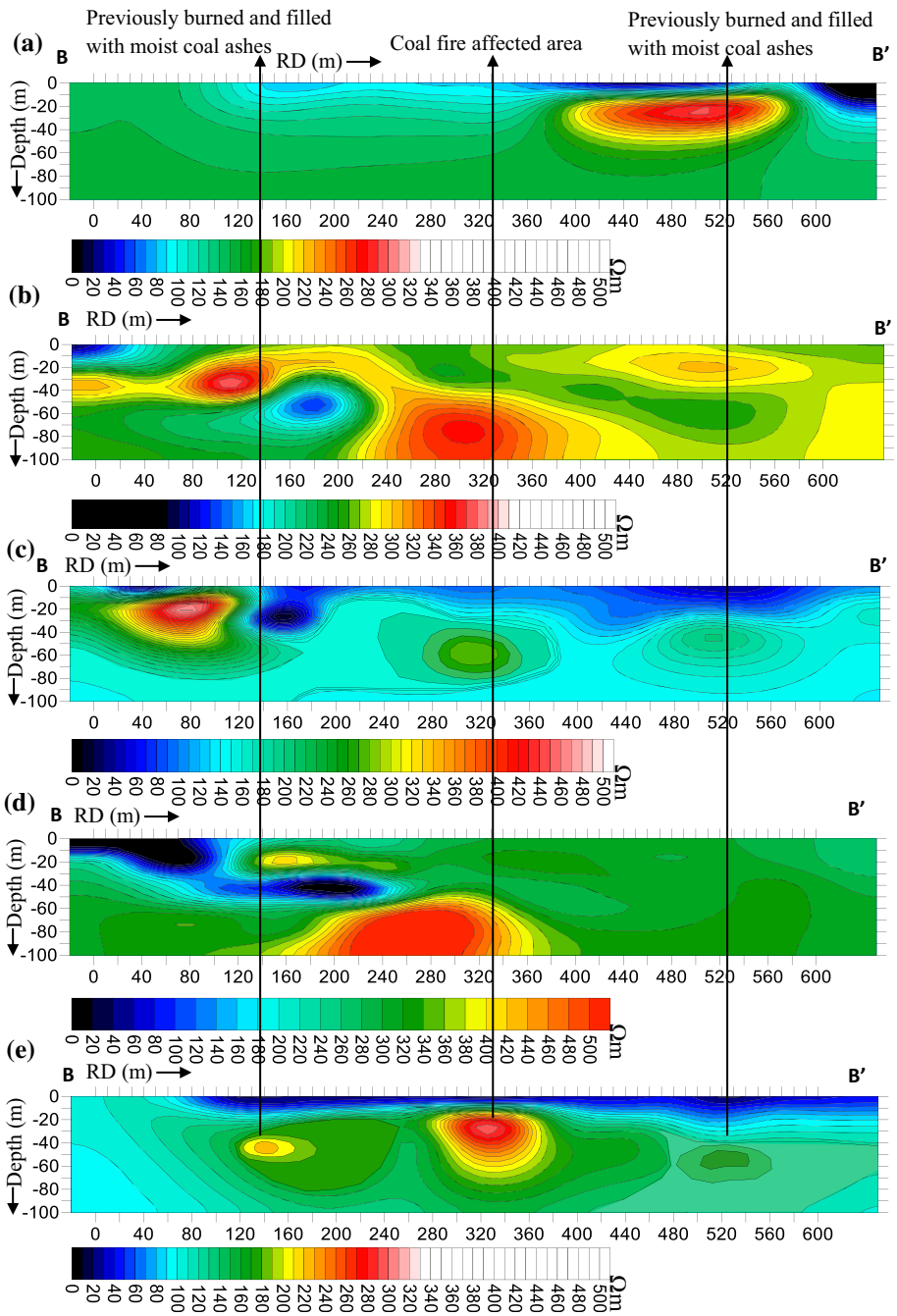

Fig. 11 2D ERT section along BB′ using **a** Wenner, **b** Schlumberger, **c** gradient, **d** dipole–dipole arrays and **e** joint inversion of all the arrays with current threshold of 60 mA and quality factor 5

Table 1 Details of distinct resistive anomalous features delineated in AA′ profile using (a) Wenner, (b) Schlumberger, (c) gradient, (d) dipole–dipole arrays, and (e) joint inversion of all the arrays corresponding to different current threshold and quality factor

2D ERT section	Reduced distance (RD in m)	Depth (m)	Inverted resistivity (Ωm)	RMS error
Current threshold of 10 mA and quality factor 17				
Wenner	120	15	160	0.693
	490	19	125	
Schlumberger	121	15	140	0.783
Gradient	95	6	163	0.703
	450	23	98	
	593	16	105	
Dipole–dipole	112	13	120	0.75
Joint inversion	91	20	187	0.599
Current threshold of 40 mA and quality factor 12				
Wenner	121	16	160	0.574
	488	17	128	
Schlumberger	121	15	155	0.572
	490	21	132	
Gradient	95	22	95	0.522
	486	26	110	
	619	22	123	
Dipole–dipole	105	14	142	0.553
Joint inversion	85	19	406	0.191
	244	43	236	
	443	52	235	
Current threshold of 60 mA and quality factor 5				
Wenner	116	22	187	0.389
Schlumberger	111	22	205	0.354
Gradient	101	22	183	0.248
	307	34	72	
	595	16	92	
Dipole–dipole	95	19	228	0.261
	302	40	85	
	595	17	93	
Joint inversion	89	25	302	0.086
	278	46	184	
	595	24	184	

delineated at depth of about 45–54 m is caused by XIV coal seam fire. These observations support the conceptual model of void formation caused by coal fire (Fig. 3). Finally, a model (Fig. 13) of fire propagation has been established by correlating different equivalent anomalous resistivity zones/cavities between the profiles AA′ and BB′ using 2D ERT sections obtained from joint inversion of all combine arrays. The coal seam-XIVA affected by fire is resulted in void at RD 89 m and at depth of 25 m (profile AA′) which is characterized by relatively high resistivity of about 300 Ωm. This fire activity is assumed to be connected with the profile BB′ at RD 324 m and at depth of 25 m through fracture plane. It is interesting to mention that coal fire smokes have been observed on the ground near RD 89 m and RD 324 m of profiles AA′ and BB′, respectively. The surface manifestation of coal fire smokes support the model established in Fig. 13. In addition, a distinct anomalous resistive zone of about 200 Ωm has been delineated at RD 278 m and at depth of 46 m (XIV seam coal, Fig. 2) in profile AA′ which is assumed to be connected with the profile BB′ at RD 520 m and at depth of 48 m through fracture plane. This zone is assumed to be previously burned and filled with moist coal ashes. Similar, anomalous resistive zones with resistivity of about 200 Ωm have been delineated, one at RD 595 m and at depth of 24 m in profile AA′ and another at RD 126 m and at depth of 44 m in profile BB′.

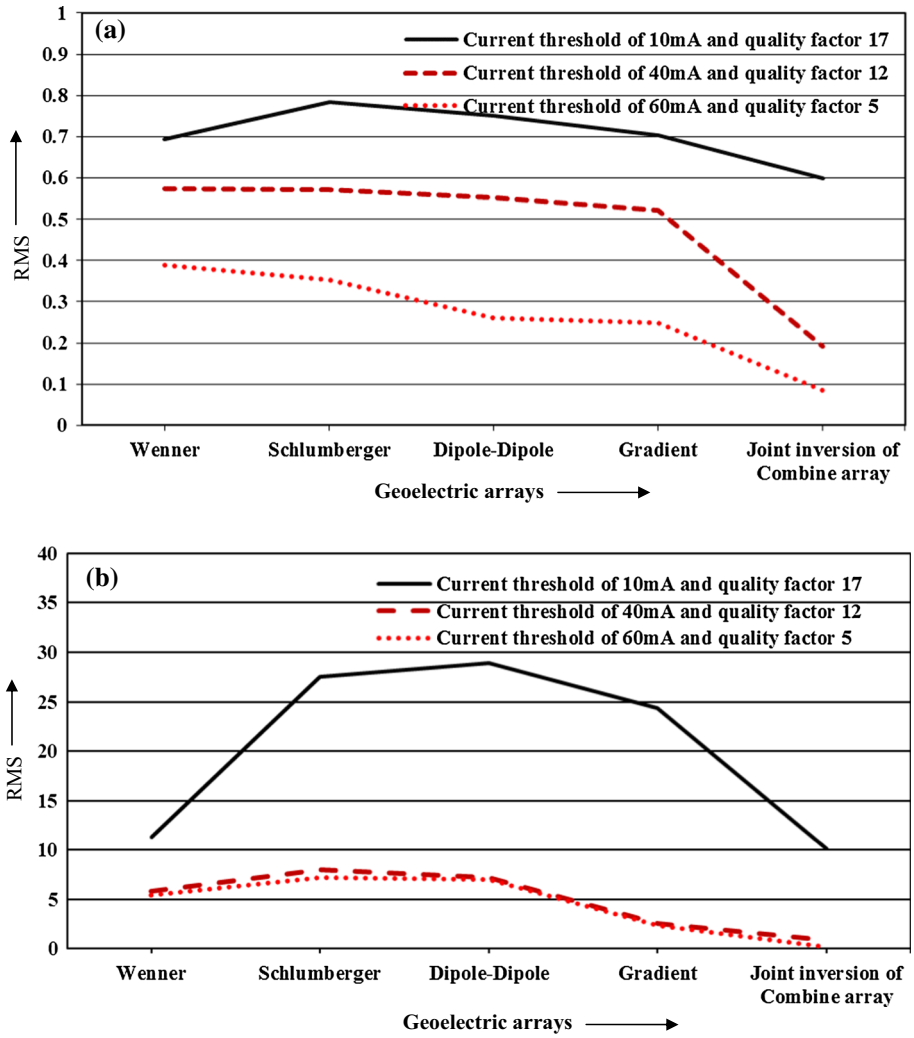

Fig. 12 Comparison of root-mean-square (RMS) error of inversion results obtained from Wenner, Schlumberger, gradient, dipole–dipole arrays and four combine array for different current threshold and data quality factor

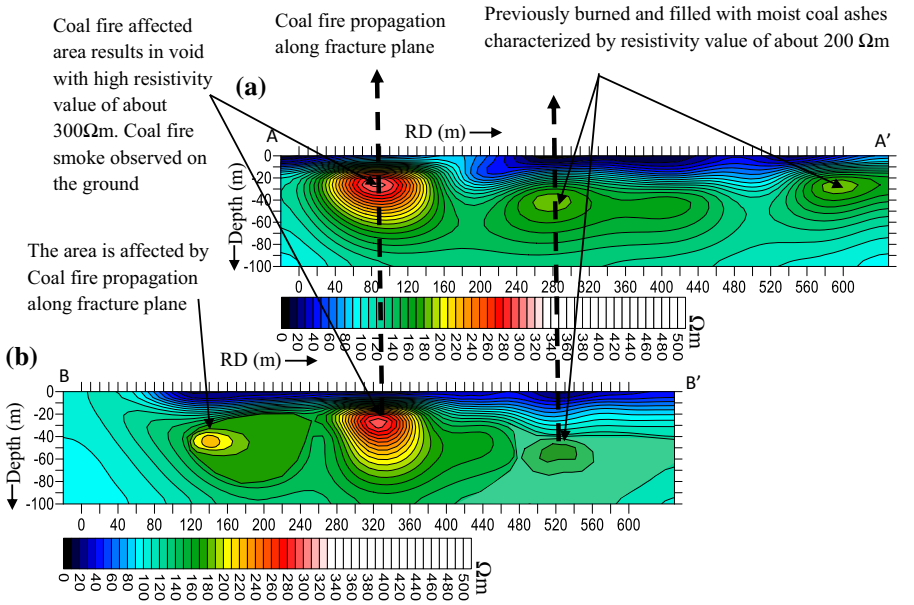

Fig. 13 Model of fire propagation and relationship of anomalous resistivity zones/cavities established from 2D ERT section of profile **a** AA′and **b** BB′using joint inversion of all the arrays with current threshold of 60 mA and quality factor 5

Table 2 Details of distinct resistive anomalous features delineated in BB′ profile using (a) Wenner, (b) Schlumberger, (c) gradient, (d) Dipole–dipole arrays and (e) joint inversion of all the arrays corresponding to different current threshold and quality factor

2D ERT section	Reduced distance (RD in m)	Depth (m)	Inverted resistivity (Ωm)	RMS error
Current threshold of 10 mA and quality factor 17				
Wenner	245	31	75	11.361
	365	34	170	
	520	18	476	
Schlumberger	102	25	465	27.56
	176	49	12	
	230	20	435	
	299	76	415	
Gradient	134	48	283	24.322
	233	63	155	
	317	53	197	
	511	46	198	
Dipole–dipole	228	90	401	28.927
Joint inversion	71	33	470	10.142
	234	44	796	
	422	32	302	
Current threshold of 40 mA and quality factor 12				
Wenner	500	22	300	5.852
Schlumberger	109	30	490	7.97
	176	54	10	
	305	72	400	
	490	60	230	
	506	20	314	
Gradient	73	17	466	2.549
	156	22	26	
	314	56	290	
	512	46	200	
Dipole–dipole	161	18	407	7.175
	195	40	10	
	267	81	570	
	372	19	330	
Joint inversion	111	40	195	0.878
	325	34	247	
	519	51	198	
Current threshold of 60 mA and quality factor 5				
Wenner	500	20	290	5.452
Schlumberger	110	34	375	7.169
	178	51	133	
	304	77	353	
	491	20	301	
Gradient	77	19	468	2.348
	159	23	24	
	316	57	298	
	511	47	199	
Dipole–dipole	157	20	407	6.998
	188	38	21	
	269	79	571	
Joint inversion	126	44	238	0.175
	324	25	294	
	520	48	185	

Conclusions

The ERT study has been carried out for delineation of hidden near-surface cavities over known coal fire affected area. Initially, field situations have been simulated for two voids with varying resistivity through forward modeling for gradient and dipole–dipole arrays. The data for both the arrays have been corrupted by 5 % random noise. The inversion of the noise corrupted data sets for both the arrays bring up the location and dimension of the voids within reasonable accuracy unlike their resistivities. Infact, the considered resistive void seems to be relatively conducting void.

Subsequently, 2D ERT data have been acquired along two profiles over coal fire affected area of Patherdih colliery using Wenner, Schlumberger, dipole–dipole, and gradient arrays. The acquired field data have been analyzed for three different combinations of quality factor and current threshold i.e. (1) 5 and 60 mA, (2) 12 and 40 mA, and (3) 17 and 10 mA, respectively. The minimum RMS error has been obtained with the quality factor 5 and threshold 60 mA for all the arrays including joint inversion of all combine arrays. In accordance with the synthetic model study, the location and dimension of the voids have been well identified using field ERT data except their resistivities. It has been established that the different resistive anomalous features delineated in both profiles are generated by burning of coal seams XIVA and XIV which leads to the void formation at the depths of about 23–25 and 45–54 m, respectively. The obtained results matches well with the available borehole log and surface manifestation of fire over the study area. These observations support the conceptual model (Fig. 3) of void formation caused by coal fire and final model of fire propagation (Fig. 13). The results proves the efficacy of the ERT technique for detection of voids associated with coal fire.

Acknowledgments Authors are thankful to DST for funding a project (SB/S4/ES-640/2012) on geotechnical characterization of Jharia coal field area using Geophysical techniques. Authors wish to thank to the Department of Science of Technology (project no. SR/FST/ESI-104/2010) and University Grant Commission (project no. F.560/1/CAS/2009(SAP-I)) Govt. of India, for using instrumental facilities under these projects. We are also thankful to the Editor and anonymous Referees for their suggestions for improvement of the manuscript. The authors wish to thank to Director, ISM and HOD, Department of Applied Geophysics, ISM, Dhanbad for their support in this study.

References

Abu-Shariah MII (2009) Determination of cave geometry by using a geoelectrical resistivity inverse model. Eng Geol 105:239–244

Bharti AK, Pal SK, Vaish J (2014) Application of self-potential method for coal fire detection over Jharia Coal field. In: 51st annual convention of Indian Geophysical Union, Kurukshetra University, Kurukshetra, 19–21 November 2014, pp 59–62

Bharti AK, Pal SK, Priyam Piyush, Narayan Satya, Pathak VK, Sahoo SD (2015) Detection of illegal mining over Raniganj Coalfield using electrical resistivity tomography. J Eng Geol Spec Pub 65–69

Brown WA, Stafford KW, Shaw-Faulkner M, Grubbs A (2011) A comparative integrated geophysical study of Horseshoe Chimney Cave, Colorado Bend State Park, Texas. Int J Speleol 40(1):9–16

Cardarelli E, Di Filippo G, Tuccinardi E (2006) Electrical resistivity tomography to detect buried cavities in Rome: a case study. Near Surf Geophys 4:387–392

Cardarelli E, Cercato M, Cerreto A, Di Filippo G (2010) Electrical resistivity and seismic refraction tomography to detect buried cavities. Geophys Prospect 58:685–695

Cardarelli E, Cercato M, De Donno G, Di Filippo G (2014) Detection and imaging of piping sinkholes by integrated geophysical methods. Near Surf Geophys 12:439–450

Chandra D (1992) Jharia Coal fields. Geological Society of India, Bangalore, p 149

Dahlin T, Zhou B (2004) A numerical comparison of 2D resistivity imaging with ten electrode arrays. Geophys Prospect 52:379–398

Dahlin T, Zhou B (2006) Multiple-gradient array measurements for multichannel 2D resistivity imaging. Near Surf Geophys 4:113–123

Duba A (1977) Electrical conductivity of coal and coal char. Fuel 56:441–443

Ezersky M (2008) Geoelectric structure of the Ein Gedi sinkhole occurrence site at the Dead Sea shore in Israel. J Appl Geophys 64:56–69. doi:10.1016/j/jappgeo.12.003

FlashRES Universal User manual (2014) ZZ Resistivity Imaging Pty Ltd, Australia, p 36

Gambetta M, Armadillo E, Carmisciano C, Stefanelli P, Cocchi L, Tontini FC (2011) Determining geophysical properties of a near surface cave through integrated microgravity vertical gradient and electrical resistivity tomography measurements. J Cave Karst Stud 73(1):11–15

Guérin R, Baltassat JM, Boucher M, Chalikakis K, Galibert PY, Girard JF, Plagnes V, Valois R (2009) Geophysical characterisation of karstic networks. Application to the Ouysse system (Poumeyssen, France). Comptes Rendus Geosci 341:810–817

Jiang L, Lin H, Ma J, Kong B, Wang Y (2011) Potential of small-baseline SAR interferometry for monitoring land subsidence related to underground coal fires: Wuda (Northern China) case study. Remote Sens Environ 115:257–268

Kumar S, Pal SK, Vaish J, Shalivahan (2015) Utilization of magnetic gradient method for coal fire mapping of Chatabad Area, a Part of Jharia Colafield, India. J Eng Geol Spec Pub 170–176

Lange AL (1999) Geophysical studies at Kartchner Caverns State Park, Arizona. J Cave Karst Stud 61(2):68–72

Leucci G, De Giorgi L (2010) Microgravity and ground penetrating radar geophysical methods to map the shallow karstic cavities network in a coastal area (Marina Di Capilungo, Lecce, Italy). Explor Geophys 41:178–188

Loke MH (1999) Electrical imaging surveys for environmental and engineering studies. A practical guide to 2-D and 3-D surveys, p 63

Martínez-Moreno FJ, Pedrera A, Ruano P, Galindo-Zaldívar J, Martos-Rosillo S, González-Castillo L, Sánchez-Úbeda JP, Marín-Lechado C (2014) Combined microgravity, electrical resistivity tomography and induced polarization to detect deeply buried caves: Algaidilla cave (Southern Spain). Eng Geol 162:67–78

Martínez-Pagán P, Gómez-Ortiz D, Martín-Crespo T, Manteca JI, Rosique M (2013) The electrical resistivity tomography method in the detection of shallow mining cavities. A case study on the Victoria Cave, Cartagena (SE Spain). Eng Geol 156:1–10

Metwaly M, AlFouzan F (2013) Application of 2-D geoelectrical resistivity tomography for subsurface cavity detection in the eastern part of Saudi Arabia. Geosci Front 4:469–476

Mochales T, Casas AM, Pueyo EL, Pueyo O, Román MT, Pocoví A, Soriano MA, Ansón D (2008) Detection of underground cavities by combining gravity, magnetic and ground penetrating radar survey: a case study from the Zaragoza area, NE Spain. Environ Geol 53:1067–1077

Pal SK, Vaish J, Kumar S, Bharti AK (2016) Coalfire mapping of East Basuria Colliery, Jharia coal field using Vertical Derivative Technique of Magnetic data. J Earth Syst Sci 125(1):165–178

Pánek T, Margielewski W, Táborik P, Urban J, Hradecký J, Szura C (2010) Gravitationally induced caves and other discontinuities detected by 2D electrical resistivity tomography: case studies from the Polish Flysch Carpathians. Geomorphology 123:165–180

Revil A, Karaoulis M, Srivastava S, Byrdina S (2013) Thermoelectric self-potential and resistivity data localize the burning front of underground coal fires. Geophysics 78(5):B259–B273

Rodríguez Castillo R, Reyes Gutierrez R (1992) Resistivity identification of shallow mining cavities in Real del Monte, México. Eng Geol 33:141–149

Singh BB, Srivardhan V, Pal SK, Kanagaraju SK, Kumar S, Vaish J (2015) Particle swarm optimization inversion of self potential anomaly for detecting coal fires, a case study - Jharia Coal Field. Third sustainable earth and sciences conference in Celle, Germany, EAGE, 13 October. doi:10.3997/2214-4609.201414282

Song Z, Kuenzer C (2014) Coal fires in China over the last decade: a comprehensive review. Int J Coal Geol 133:72–99

Srivardhan V, Pal SK, Vaish J, Kumar S, Bharti AK, Priyam P (2016) Particle swarm optimization inversion of self-potential data for depth estimation of coal fires over East Basuria colliery, Jharia coalfield, India. Environ Earth Sci (**in press**)

Stummer P, Maurer H, Green A (2004) Experimental design: electrical resistivity data sets that provide optimum subsurface information. Geophysics 69:120–139

Vaish J, Pal SK (2013) Interpretation of Magnetic Anomaly data over East Basuria region using an Enhanced Local Wavenumber (ELW) Technique. In: 10th Biennial International conference and exposition on petroleum geophysics, Kochi, 23–25 November, p 110

Vaish J, Pal SK (2015a) Subsurface coal fire mapping of East Basuria Colliery, Jharkhand. J Geol Soc India 86(4):438–444

Vaish J, Pal SK (2015b) Geological mapping of Jharia Coalfield, India using GRACE EGM2008 gravity data: a vertical derivative approach. Geocarto Int 30(4):388–401

Vaish J, Pal SK (2016) Subsurface Coal fire mapping of Patherdih Colliery a part of Jharia coal field, India. J Geol Soc India (**in press**)

Valois R, Bermejo L, Guérin R, Hinguant S, Pigeaud R, Rodet J (2010) Karstic morphologies identified with geophysics around Saulges caves (Mayenne, France). Archaeol Prospect 17:151–160

Van Schoor M (2002) Detecting of sinkholes using 2D electrical resistivity imaging. J Appl Geophys 50:393–399

Verma RK, Bhuin NC (1979) Use of electrical resistivity methods for study of coal seams in parts of the Jharia Coalfields, India. Geoexploration 17:163–176

Verma RK, Bandopadhyay TK, Bhuin NC (1982) Use of Electrical resistivity methods for the study of coal seams in parts of the Raniganj Coalfields (India). Geophys Prospect 30:115–126

Zhe J, Greenhalgh S, Marescot L (2007) Multichannel, full waveform and flexible electrode combination resistivity-imaging system. Geophysics 72(2):57–64. doi:10.1190/1.2435081

Zhou B, Greenhalgh SA (2000) Crosshole resistivity tomography using different electrode configurations. Geophys Prospect 48:887–912

Zhou QY, Matsui H, Shimada J (2004) Characterization of the unsaturated zone around a cavity in fractured rocks using electrical resistivity tomography. J Hydraul Res 42:25–31